2 CSL Data Processing and Interpretation Using 3-D Tomography

Tomography is a generic term that technically means to "draw an image or a section" of a target material. The first concept of tomography originated in the medical field where CAT (computer aided tomography) scans have become standard practice. Research for adapting tomography to more restrictive geometries encountered in the geotechnical field has accelerated since Devaney (1980) introduced geophysical diffraction tomography. Since then, 3-D tomographic imaging methods have been used worldwide in the geotechnical and geological fields. Geotechnical imaging capabilities with tomographic methods have been significantly improved in recent years and expanded to accurately characterize the subsurface and to detect underground cavities, geological anomalies, and subsurface discontinuities.

2.1 Basic Principles for 3-D Tomography

The basic principles of tomography are borrowed from the medical field where imaging of a body is done by multidirectional CAT-scans. Tomography for medical purposes is used to display the loss in intensity of x-rays due to absorptive properties of different body parts. Because x-ray imaging depends entirely on variations in absorption with no refraction or diffraction, medical and seismic tomography are not perfectly analogous. In CAT-scanning, the x-rays travel mostly in straight lines in many directions, whereas in seismic tomography, the ray paths can bend appreciably depending on the velocity contrast within the medium.

The main concept of 3-D seismic tomographic imaging is the creation of color-coded images that provide a clear and detailed representation of property variations within a medium from seismic rays projected through the medium. Travel time tomography involves imaging the seismic properties from the observation of the transmitted

compressional first arrival energy (Dines and Lytle, 1979). The relationship between the travel time t_i and the velocity field $v_{(x,y)}$ is given by the line integral for a ray "i":

$$t_i = \int_{R_i} \frac{ds}{v_{(x,y)}} \tag{2.1}$$

where

ds is the path length,

R_i denotes the curve connecting a source receiver pair that yields the least possible travel time according to Fermat's principle.

Tomography is an attempt to match calculated travel times from model responses to the observed data by inversion of these line integrals. Initially, the region of interest is divided into grids of uniform cells "j" of constant velocity cells and a discrete approximation of the line integral is assumed as:

$$t_i = \sum_j \Delta S_{ij} . n_j \tag{2.2}$$

where

ΔS_{ij} is the distance traveled by ray "i" in cell "j"

n_j is the slowness (inverse of velocity) within cell "j".

Using a first order Taylor expansion and neglecting residual error, from equations (2.1) and (2.2), the following equation can be written in matrix form as:

$$\bar{y} = A\bar{x} \tag{2.3}$$

where

$\bar{y}$ is the difference between computed travel times obtained from the model and the observed travel times obtained from the field

$\bar{x}$ is the difference between the true and the modeled slowness

A is the Jacobian matrix.

In travel time tomography, Equation 2.3 is usually solved by two methods: 1)- the matrix inversion approach (e.g. conjugate gradient (CG) matrix inversion technique) (Nolet, 1987; Scales, 1987); and 2)- the "back-projection" inversion technique, adapted from medical tomography (e.g. simultaneous iterative reconstruction technique (SIRT)) (Herman, 1980; Ivanson, 1986).

In both techniques, the acoustic wave-field is initially propagated through a presumed theoretical model, and a set of travel times are obtained by ray tracing through the cells (forward modeling step). The travel time equations are then inverted iteratively to solve for the changes in slowness that produces a best-fit solution with the lowest root mean square (RMS) error between the observed and computed travel times (inversion step). The model is then modified, new ray paths traced, and the process repeated until the slowness distribution matches observations within acceptable tolerances. In practice, an adequate tomographic solution can be obtained if enough ray paths penetrate the medium in multiple directions. To reach this, the recording procedure uses large number of source/receiver locations. Color-coded tomograms of the velocity distribution within the medium are then generated from inversion results as the final step in the tomography data processing. Tomogram interpretation is the next step for defining areas of defects by evaluating velocity changes through the medium (Robert E. Sheriff and Lloyd P. Geldart, 1995).

In velocity tomography, only the first arrival pulses are considered. Therefore, only the signal component that travels through the fastest path is used in the analysis. As the velocity changes through the medium due to energy absorption, the slowness (1/velocity) of any uniform cell of the medium may change not only the travel time, but also the ray path.

A number of software algorithms for performing travel time tomography exist. These algorithms utilize straight or curved rays, 2-D or 3-D matrix inversion, and 2-D or 3-

D graphic packages to display the results. For accurate volumetric imaging of anomalies in drilled shafts, it is critical to use a software package with the following characteristics: a)- curved ray tracing or wave propagation; b)- true 3-D tomographic inversion; c)- 3-D display of data. Two-dimensional tomographic inversion produces defect images in 2-D planes (panels), which is inadequate for reconstructing the size and shape of anomalies in some cases.

2.2 Case Studies

CSL data obtained from several drilled shafts constructed for two bridges were re-processed in 3-D using RockVision3D (developed by NSA Engineering) tomographic imaging software. This software incorporates the simultaneous iterative reconstruction process (SIRT) to converge the solution set to a range of values within operator-specified limits. The program has the capability for mesh initialization, data filtering and processing, and reconstruction of tomograms.

Velocity tomograms were produced using the curved-ray method to obtain results with highest accuracy. The curved-ray technique used in the RockVision3D software computes the node value using the steepest descent on the travel-time mesh, nearly matching the computational efficiency of the straight-ray technique. Shooting curved-rays from the source to the receiver using a pixel-based mesh occasionally encounters problems such as shadow zones. Use of a node-based mesh rather than a pixel-based mesh eliminates these inconsistencies. CSL seismic signals are picked, analyzed, and processed to derive velocity tomographic images. A velocity tomogram is created from measuring the time it takes for each ray to travel through the medium from the source to receiver. Typically areas of relatively higher velocity generally correspond to areas of more competent or consolidated material, whereas areas of relatively lower velocity represent zones of less consolidated or medium to

soft material. Once the velocity tomogram is calculated, 2-D cross-sections or 3-D velocity contours can be displayed.

Two sites are selected to evaluate the effectiveness of implementing 3-D tomographic imaging methods on CSL field data to accurately define the geometry and location of anomalous areas within a drilled shaft. The results were also used to propose a plan for corrective action, and to determine the effectiveness of the recommended corrective plan.

2.2.1 Bridge Foundation Construction Site 1

At this site, two larger diameter concrete casings of approximately 1.525 m and 1.675 m diameter were installed extending to the top of bedrock, and the annular space between the casings was filled with sand to accommodate seismic design requirements.

During the subsurface characterization, three borings were advanced below the bridge foundation. The following describes the materials encountered in each of the borings:

- Boring B-5 was advanced at the left side of the proposed abutment 2 location as shown in Figure 2.1a. This boring encountered sandy gravel with cobbles and boulders from 0 to 6.9 m deep and sandstone from 6.9 to 11.4 m deep.
- Boring B-6 was advanced at the left side of the proposed abutment 1 location as shown in Figure 2.1b. This boring encountered sandy gravel with cobbles and boulders from 0 to 4.05 m deep and sandstone from 4.05 to 8.7 m deep.

(a)

(b)

(c)

Figure 2.1 Pictures Showing Locations of (a) Boring B-5, (b) Boring B-6, and (c) Boring B-7

- Boring B-7 was advanced on the right side of the proposed pier location shown in Figure 2.1c. This boring encountered sandy gravel with cobbles and boulders from 0 to 1.2 m deep and sandstone from 1.2 to 6.6 m deep.

The subsurface profiles from each boring and borehole location with respect to the new bridge design are summarized in Figure 2.2.

The drilled shafts for the bridge at this site have a diameter of 915 mm and lengths ranging from 6.3 m to 10.0 m. The drilled shafts were socketed 3 m into bedrock with permanent corrugated steel casing extending to the tops. Three 50 mm diameter steel CSL access tubes were attached to the inside of the reinforcing rebar cages extending approximately 75 mm above the bottom of the shafts. The horizontal spacing between adjacent tubes at the tops of the shafts was typically within 440 mm to 640 mm. The drilled shaft details are presented in Figure 2.3.

2.2.1.1 CSL Test Procedures

Cross-hole sonic logging for all eight drilled shafts at abutments 1 and 2 were conducted by GRL using a PISA-CHUM ultrasonic pulse analyzer system. The CSL results consisted of x,y plots of first arrival times (FAT) of the P-wave and "relative energy" versus depth. The plots are presented in Appendix A. The PISA-CHUM system plots the unitless "relative energy" rather than "absolute energy". This is due to the fact that transmitted energy, signal frequency, and signal transit distance have an effect on absolute energy values. These parameters are mainly related to the test procedure and equipment and not to the concrete quality; therefore, no useful data are given. Relative energy values, on the other hand, are cased by changes within the tested medium and are, therefore, a better indication of shaft quality.

Figure 2.2 Schematic of Site 1 Bridge Plan and Subsurface Profile

67

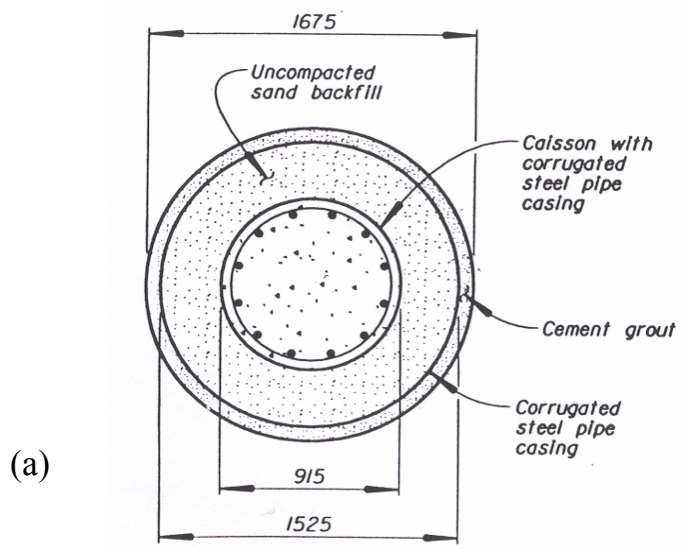

(a)

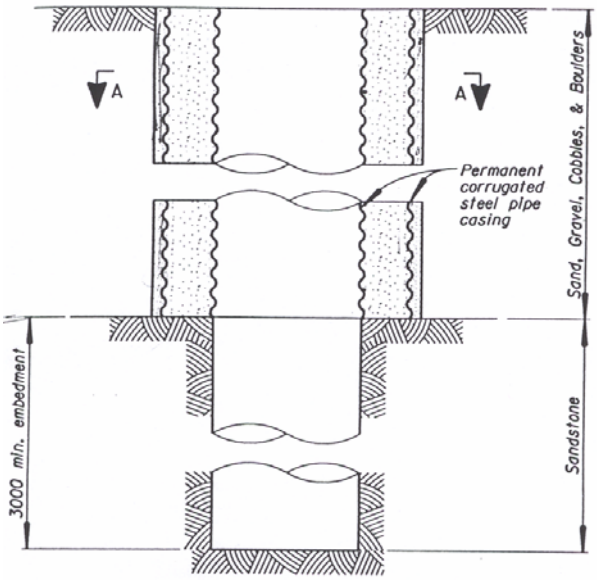

(b)

Figure 2.3 Drilled Shaft, (a) Horizontal Cross-Section, (b) Vertical Cross-Section

Prior to testing each shaft, the CSL access tube lengths and the horizontal spacing between the tubes (at the top of shafts) were accurately measured and recorded. Each of the three tube pair combinations (1-2, 2-3, and 1-3) was logged once with the CSL probes pulled at equal rates at the same horizon. The data (FAT) was immediately evaluated, and if a uniform data log was indicated, it was assumed that no defects existed between the tested pair, and testing proceeded to the next pair of tubes. If a significant data anomaly was depicted, the test was repeated between the same pair for reproducibility. If the time delays were still apparent, the cross-section was typically re-logged using probe vertical offsets of 0.5 m and 1.0 m. This was only necessary on shaft A1-2 (shaft number 2 in Abutment 1) for the tube pair 1-2, as will be discussed further. Shaft installation and CSL equipment setup is shown on Figure 2.4.

Slight differences between the length of meaningful CSL data and the computed length of concrete often occur. These differences are due to loss of CSL signal near the top of the drilled shaft and due to imprecision or occasional slippage in the depth recording apparatus. The CSL records near the top section of the shaft are often not reliable for evaluating concrete quality and cannot be used to precisely delineate the upper extent of the shaft surface. The reasons for this will be discussed further in the report. During field logging, data were always recorded from the bottom of the tubes to some elevation above the concrete. Only data along the concrete length are plotted, and all other data are removed.

The average FAT and velocity were computed for each cross-sectional log using data from the entire scan (excluding the top 0.5 m). To quantify abrupt signal delays in a scan, the maximum percent reduction in velocity over 1 m length interval was calculated by dividing the minimum average velocity for any five-centimeter interval by average velocity for a 1 m interval, above and below that location. This was done primarily to conform to the project concrete defect criteria listed in the specifications,

(a) Drilling Before Shaft Installation

(b) Casing Installation

(c) Abutment with four Drilled Shafts

(d) CSL Measurements

Figure 2.4 Drilled Shaft Installation and CSL Measurements

which require that the drilled shafts be assigned a concrete condition rating based on percent wave velocity reduction (discussed earlier in this report).

2.2.1.2 CSL Test Results and Analysis

The CSL data were plotted (Appendix A) and analyzed according to the concrete rating criteria (CRC). Summaries of the results are shown in Table 2.1. The CSL results from all eight shafts except for shaft A1-2 produced relatively uniform scanswith FAT delays and relative energy reductions of less than 10%. These scans are categorized as Good (G) as defined in the concrete condition rating criteria. The average velocities (excluding top 0.5 m) for all scans ranged from 3,149 to 4,047 m/s with an overall average of 3,495 m/s

For shaft A1-2, tube pair 1-2 yielded a signal delay and reduced energy zone approximately 1.5 to 2.5 m from the bottom of the shaft. Repeated CSL between tube pairs 1-2 with the probes vertically offset gave similar results. On-site data evaluation indicated that the maximum signal delay was between 15% and 25% greater than the average, which results in either a Questionable (Q) or Poor/Defect (P/D) rating based on concrete condition criteria. Further review and analysis of the first arrivals indicated the average arrival time for all data points in tube pair 1-2 in shaft A1-2 was 0.187 ms. Based on the nominal tube spacing of 0.78 m at the top of the shaft, the average calculated velocity for this scan is 4,171 m/s. The average of ten data points including and surrounding the longest arrivals time was 0.223 ms, yielding a maximum signal delay of 19%. This zone of maximum signal delay was located approximately 2 m from the bottom of the shaft and was re-classified as a Questionable zone (Q) according to the rating criteria.

The signal delay could be caused by a horizontal defect that may exist between tubes 1 and 2. Also, the increased travel distance for the offset scans may have decreased

Table 2.1 CSL Results from the Eight Shafts at Abutments 1 and 2, Site 1

Abut. Shaft #	Tube Pairs	Age, days	L, m	S, m	FAT, ms	V_{ave}, m/s	V_{max} Red. %	Depth % Red. m	Depth V_{min},)	CRC
A1-1	1-2	14	5.6	0.60	167	3594	4.0	0.4	4.6	G
A1-1	2-3	14	5.6	0.63	186	3397	5.1	1.9	4.3	G
A1-1	1-3	14	5.6	0.44	140	3149	4.3	4.3	4.7	G
A1-2	1-2	12	5.6	0.60	185	3269	19.0	2.1	2.1	Q
A1-2	1-2os.5	12	5.1	0.78	236	3329	11.0	2.0	2.0	Q
A1-2	12os.1	12	4.9	1.17	299	3926	7.3	3.0	3.0	G
A1-2	2-3	12	5.6	0.50	169	3210	7.0	1.2	1.2	G
A1-2	1-3	12	2.6	0.60	178	3386	7.0	1.7	1.7	G
A1-3	1-2	9	5.5	0.58	176	3293	3.4	1.9	1.9	G
A1-3	2-3	9	5.5	0.57	166	3442	7.6	4.2	4.2	G
A1-3	1-3	9	5.5	0.59	175	3376	4.0	3.9	3.9	G
A1-4	1-2	13	9.4	0.53	163	3255	6.4	6.2	6.2	G
A1-4	2-3	13	9.4	0.58	183	3177	7.6	8.2	8.2	G
A1-4	1-3	13	9.4	0.56	164	3433	8.4	7.4	7.4	G
A2-1	1-2	4	8.5	0.58	164	3540	7.0	7.1	7.1	G
A2-1	2-3	4	8.5	0.55	160	3450	5.1	3.0	3.0	G
A2-1	1-3	4	8.5	0.55	164	3541	3.6	4.0	4.0	G
A2-2	1-2	13	8.4	0.53	158	3355	4.8	4.3	4.3	G
A2-2	2-3	13	8.4	0.58	160	3642	8.7	4.0	4.0	G
A2-2	1-3	13	8.4	0.58	164	3535	5.1	6.3	6.2	G
A2-3	1-2	6	8.4	0.55	165	3404	2.9	4.5	4.5	G
A2-3	2-3	6	8.4	0.64	158	4047	3.9	0.8	0.8	G
A2-3	1-3	6	8.4	0.58	169	3436	3.5	0.7	0.7	G
A2-4	1-2	11	8.2	0.58	156	3731	4.7	6.5	6.6	G
A2-4	2-3	11	8.2	0.60	154	3897	4.3	4.0	4.0	G
A2-4	1-3	11	8.2	0.63	145	4019	3.3	6.8	6.8	G

Column 1 – abutment-shaft number. A1-1 = abutment 1, shaft 1
Column 2 - access tube pair tested. 1-2 indicate test between tubes 1 and 2
Column 3 - concrete age at the time of testing
Column 4 - measured tube length to the top of concrete
Column 5 - spacing "S" between tubes on top of the shaft
Column 6 - average FAT from the entire log
Column 7 - average Velocity from the entire log (V_{ave}=S/FAT_{ave})
Column 8 - maximum % reduction in velocity over 1-m distance

Column 9 - location of maximum velocity reduction from bottom of shaft
Column 10 - location of minimum velocity from bottom shaft
Column 11 - concrete condition rating criteria, based on project specifications

the amount of error that can be caused by non-parallel transducer spacing. For example, the tubes or the rebar cage to which they are attached may shift during cage placement or concrete placement. Furthermore, the location of each probe within a 50-mm tube can deviate by 25 mm, since the probe diameter is approximately half the tube diameter. Thus, probe spacing can fluctuate by up to 50 mm depending on whether or not the probes are centered in the access tubes. For smaller tube spacing, this potential error source is higher. This factor alone can result in FAT delays of up to 8% for a tube spacing of 0.6 m, which is a typical size for these shafts. Based on the above discussions, the concrete quality rating criteria given in the specifications may be conservative and should be adjusted to consider shaft diameter and tube spacing.

2.2.1.3 Tomographic Imaging of the CSL Test Results

The CSL data measured between the three access tubes of abutment 1 shaft 2 were processed for P-wave first arrival times. The data were then processed using the RockVision3D software for generating 3-D velocity tomograms of the shaft interior. The input information for the tomogram generation was; 1) depth of the shaft where the first arrived component of the signal was measured, 2) the first picked arrived time at each depth, and 3) tube separation distance.

The program code is designed to provide multiple iterative reconstructions of path length for calculated seismic velocity determined from measured travel times. Ray paths are calculated by propagating a finite-difference wave front across the surveyed shaft from a known source location. For low velocity contrast, straight rays are often assumed. In higher velocity contrast, the rays bend (refract) resulting in longer ray paths.

A 3-D representation of the shaft interior was constructed and imaged to produce 3-D contours velocities (green areas in the figure) to emphasize areas of "questionable" integrity and 2-D cross-sections between access tubes Figure 2.5. From these images, three distinct velocity contrast zones are seen: z*one1* with maximum measured velocity (red), which indicates that the concrete is in "good" condition; z*one 2* with middle range velocity (green), indicating velocities 10%-20% lower than the maximum measured velocity, and z*one 3* upper zone (purple) showing the extent of the shaft with the velocities down to 2,000 m/s. This zone shows the top of the shaft where the tubes are outside the concrete and is not an indication of any defects in the upper area of the shaft. The locations, size, and orientation of the anomalies are clearly depicted in these images.

Horizontal cross-sections looking from the top of the shaft at 0.5-m intervals are also plotted and shown in Appendix B. The first image at 5.5 m from the bottom of the shaft shows the portion of the shaft with the velocities down to 2,000 m/s. Going deeper into the shaft, the location of an anomalous zone with the velocities of the concrete showing "questionable" structure condition can be clearly seen. Images were produced to compare the results of the CSL x,y plots with the tomographic imaging maps. By plotting color-coded 3-D tomographic images of the ultrasonic data (CSL), accurate location of anomalous/questionable zones and their geometries can result in more reliable information about the shaft concrete integrity.

2.2.2 Bridge Foundation Construction Site 2

The CSL data logs from abutment 2 shaft 4 (A2-4) indicated a significant signal delay between all tubes at a depth between 6 m and 7 m from the top of the shaft. A signal velocity delay of about 14%, 29%, and 50% was recorded between access tubes 1-2, 1-3, and 2-3, respectively. Although the CSL logs indicated an anomalous area

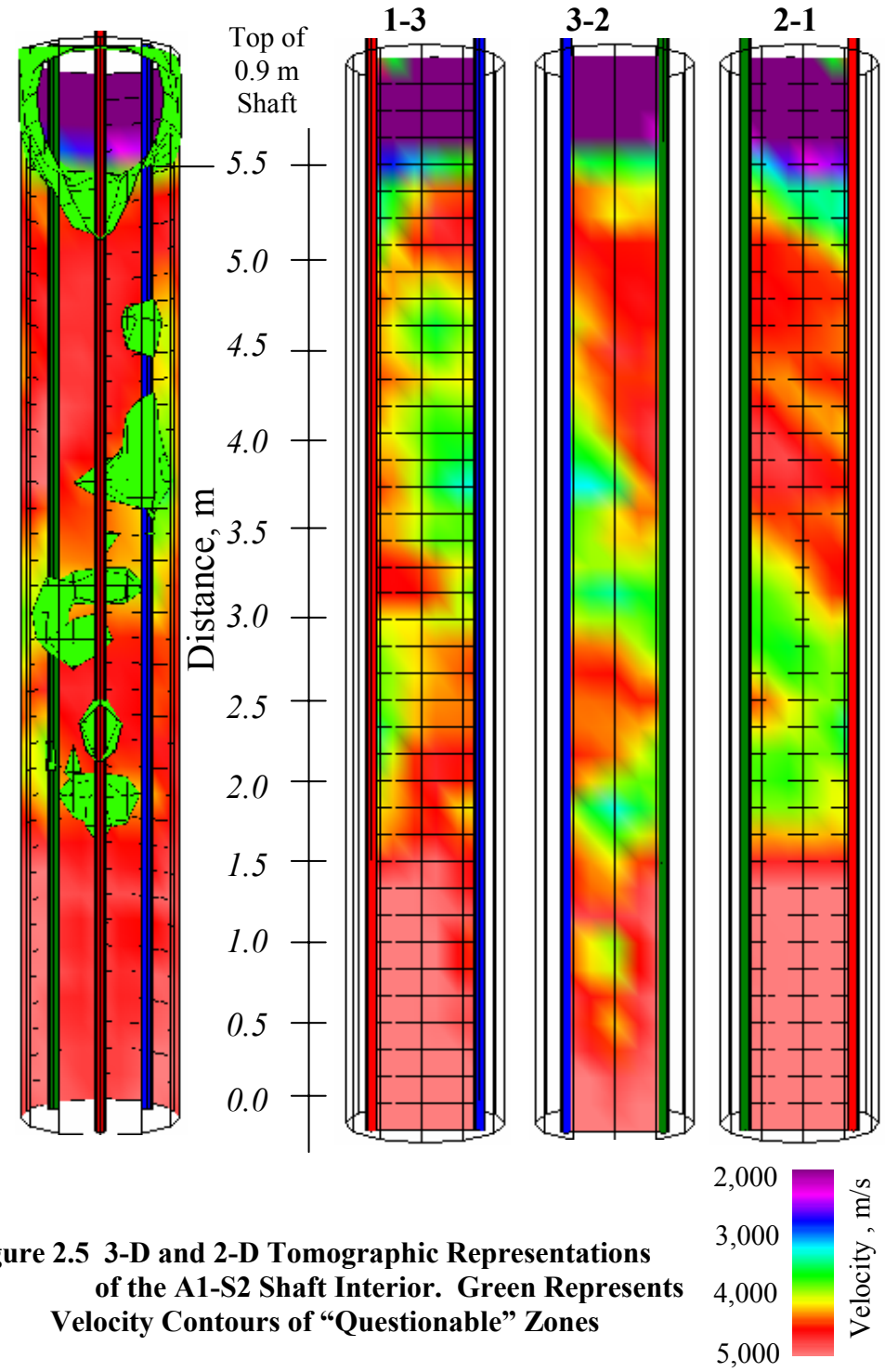

Figure 2.5 3-D and 2-D Tomographic Representations of the A1-S2 Shaft Interior. Green Represents Velocity Contours of "Questionable" Zones

within A2-4, the size, geometry, and exact location of the defect could not be determined.

Four borings were advanced for subsurface exploration. Survey results indicated that upper soils consisted of alluvial deposits of silty sand with cobbles and boulders overlaying highly fractured (decomposed) shale rock. The quality and strength of shale increased with depth.

The following are results from each boring:

- Boring B-1 was located at the proposed pier location in the right lane of the existing bridge. Boring B-1 encountered silty sandy gravel with cobbles and boulders from 0 to 5.1 m. Decomposed shale was encountered from 5.1 to 5.25 m. The bottom 1.5 m of casing was lost in the hole during extraction, and drilling was terminated.
- Boring B-2 was located at the left side of the proposed abutment 1 location. Boring B-2 encountered silty sandy gravel with cobbles from 0 to 2.7 m, and weak shale was encountered from 5.1 to 14.4 m.
- Boring B-3 was located at the left side of the proposed pier location. Boring B-3 encountered silty sandy gravel with cobbles and boulders from 0 to 5.1 m, and shale was encountered from 5.1 to 11.7 m.
- Boring B-4 was located at the right side of the proposed abutment 2 location. Boring B-4 encountered silty sandy gravel with cobbles and boulders from 0 to 5.4 m, and shale was encountered from 5.4 to 11.1 m.

The groundwater elevations are assumed to coincide with the level of the water in the stream channel below the bridge at the time of drilling. The subsurface profiles from each boring and borehole locations with respect to the new bridge design are shown in Figure 2.6.

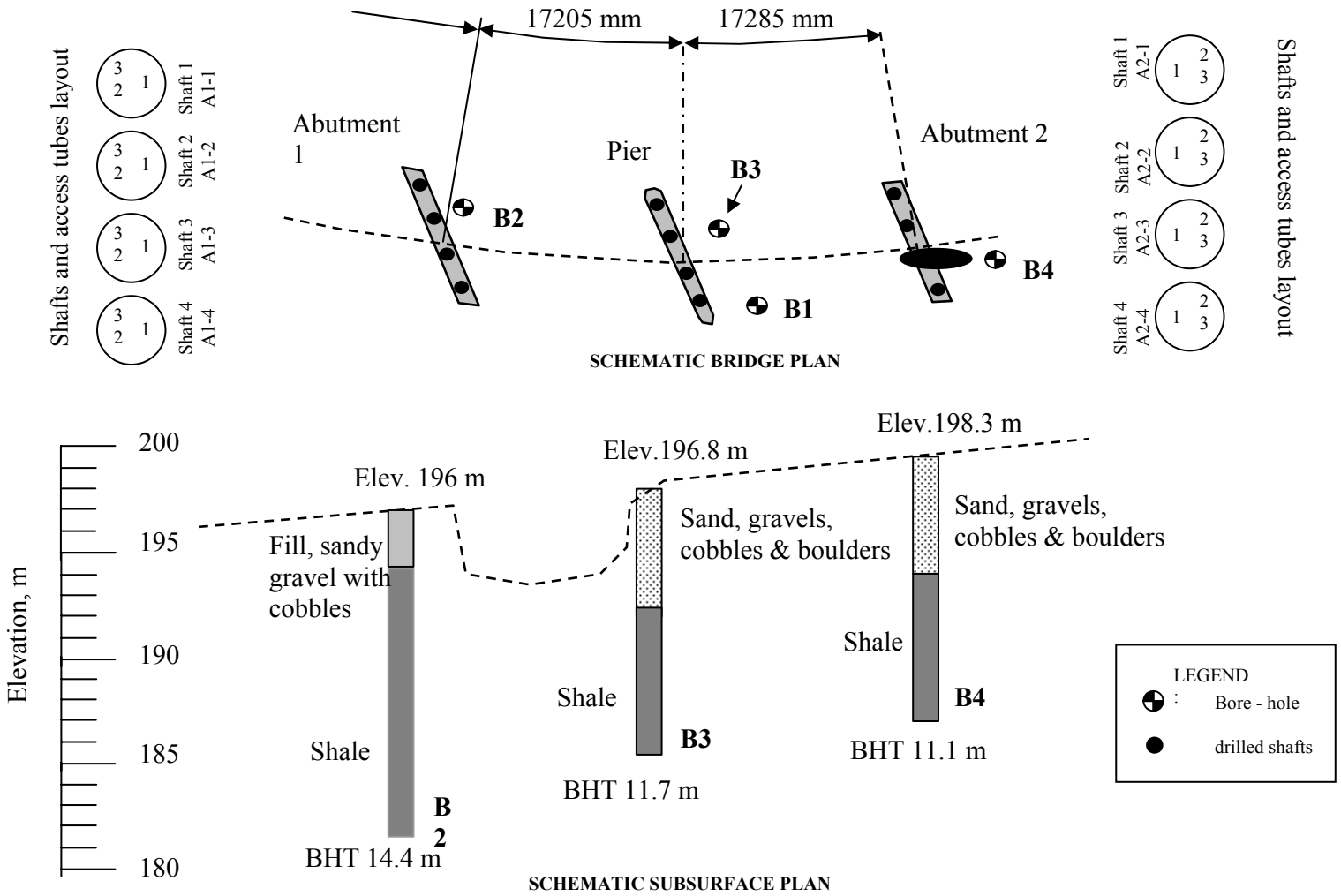

Figure 2.6 Schematic of Site 2 Bridge Plan and Subsurface Profile

The bridge is two span with four drilled shafts in each abutment and four drilled shafts in the pier. The 912-mm-diameter abutment shafts and the 1,220-mm-diameter pier drilled shafts extended to an estimated depth of about 11 m. Each shaft was drilled into rock sockets with permanent corrugated steel casing extending to the pile top. Larger diameter casings extend to the top of bedrock, and the annulus between the two casings was filled with sand. The 912-mm and 1,220-mm shafts were equipped with three and four CSL access tubes, respectively. The 50 mm diameter access tubes were attached to the inside of the reinforcing rebar cage and were extended to approximately 0.3 m above the bottoms of the shafts. The measured access tube lengths embedded in concrete ranged from approximately 8.2 m to 12.2 m. The shafts are referred to as A1-1, A1-2, A1-3, and A1-4 for abutment 1; A2-1, A2-2, A2-3, and A2-4 for abutment 2. The shafts of the central pier are referred to as CP1, CP2, CP3, and CP4. The detailed drawings for the drilled shaft casings are presented in Figure 2.7.

2.2.2.1 CSL Test Procedures

Cross-hole sonic logging for all drilled shafts at this site was performed by GRL, using a PISA-CHUM Ultrasonic Pulse Analyzer system. Prior to testing, the CSL access tube lengths and the horizontal spacing of the access tubes at the top of each shaft were accurately measured and recorded. The measured tube spacing ranged from 0.5 to 0.96 m and was used to calculate the "apparent" wave velocity. The "apparent" velocities are, therefore not direct measurements but are calculated by dividing the measured nominal tube spacing, measured at the top of the shaft, by the measured FAT. Every possible tube pair combination was logged with the probes pulled at the same horizon; thus, three logs were possible for each 912-mm-diameter shaft and six logs for each 1,220-mm-diameter shaft. During testing, the transmitter pulse was sent and received at 10-mm intervals along the length of the tube. The CSL results consisted of plots of measured first-arrival times (FAT) of the P-wave,

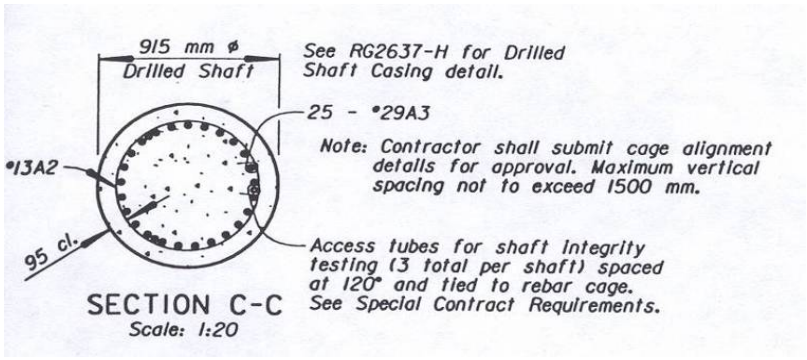

(a)

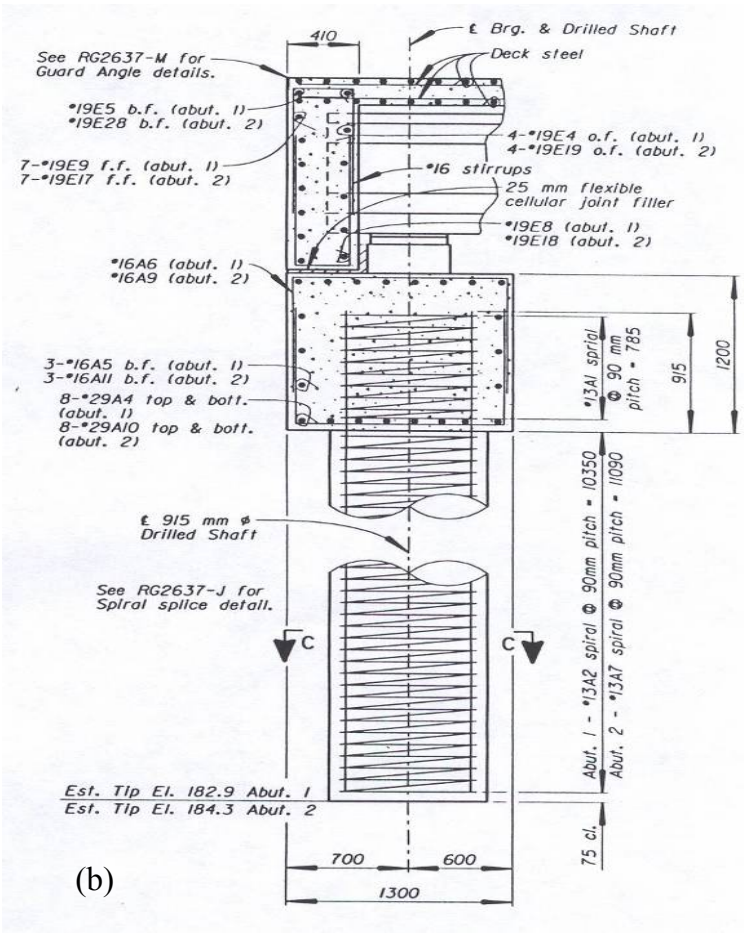

(b)

Figure 2.7 Drilled Shaft Details (a) Horizontal Cross-Section, (b) Vertical Cross-Section

measured “relative energy”, and calculated “apparent” velocity versus depth. A summary of all CSL data and results are shown in Table 2.2, and all plots are presented in Appendix C. The CSL logs were evaluated on-site for accuracy and uniformity. If relatively uniform logs were indicated in the field, the next tube combinations were tested. If a significant FAT delay was depicted, the test was repeated, with no probe offsets, for reproducibility. If FAT delays were apparent, the same cross-section was re-logged using probe vertical offsets of 0.5-m intervals. At this site, this was only necessary on shaft A2-4 for all tube pairs. Due to the signal delay significance, this set of tests was also repeated about two weeks later. In an attempt to better locate the anomaly and to determine if tube debonding might have affected the signal delay, a single-hole CSL test was conducted with the transducer and receiver stacked vertically at a 0.5 m offset. Unfortunately, the entire signal traveled through the water filling the tube, and the results were inconclusive. A third test was conducted at this shaft after coring and high-pressure jet grouting repairs were performed.

Table 2.2 Summary of CSL Results at Site 2

Shaft	Tube Pair / log	Test Length (m)	Tube Dist. (m)	FAT Ave (ms)	V_{avg} (m/s)	V_{max} Red. %	Depth V_{max} % M	V_{min} (m/s)	Depth V_{min} (m)	CRC
A1-1	12	10.7	0.53	148	3581.1	10	0.7	2970	0.7	G
A1-1	23	10.8	0.52	174	2988.5	5	4.3	2760	4.3	G
A1-1	13	11.0	0.55	145	3793.1	6	3.3	3526	3.3	G
A1-2	12	9.9	0.49	137	3576.6	6	2.1	3400	9.0	G
A1-2	23	10.3	0.58	153	3790.8	7	9.1	3440	9.1	G
A1-2	13	10.6	0.55	148	3716.2	7	3.8	3354	0.8	G
A1-3	12	10.1	0.55	158	3481.0	7	3.6	3274	0.0	G
A1-3	23	10.1	0.55	148	3716.2	5	3.7	3438	0.5	G
A1-3	13	10.2	0.55	163	3374.2	9	8.9	3031	1.8	G
A1-4	12	11.8	0.58	180	3222.2	5	1.6	2921	1.6	G

Table 2.2 Summary of CSL Results at Site 2

Shaft	Tube Pair / log	Test Length (m)	Tube Dist. (m)	FAT Ave (ms)	V_{avg} (m/s)	V_{max} Red. %	Depth V_{max} % M	V_{min} (m/s)	Depth V_{min} (m)	CRC
A1-4	23	11.9	0.52	145	3586.2	6	3.3	3192	2.8	G
A1-4	13	12.2	0.49	146	3356.2	5	6.0	3178	6.0	G
A2-1	12	10.5	0.46	125	3680.0	4	9.1	3235	6.1	G
A2-1	23	10.9	0.55	151	3642.4	7	2.0	3290	2.0	G
A2-1	13	10.9	0.61	167	3652.7	5	1.9	3368	1.9	G
A2-2	12	10.4	0.46	130	3538.5	5	1.3	3100	1.3	G
A2-2	23	11.3	0.55	166	3313.3	5	4.3	3093	0.0	G
A2-2	13	10.5	0.61	169	3609.5	10	6.7	3189	0.0	G
A2-3	12	11.9	0.52	142	3662.0	2	1.9	3566	1.9	G
A2-3	23	10.0	0.49	163	3006.1	7	4.6	2813	1.0	G
A2-3	13	10.0	0.55	151	3642.4	6	7.6	3346	7.6	G
A2-4	12	11.5	0.55	160	3437.5	26	6.2	2498	6.2	P
A2-4	12OF	10.6	0.55	212	2594.3	26	6.5	2508	6.5	P
A2-4	23	11.3	0.52	150	3466.7	85	6.2	<1000	6.2	P
A2-4	23OF	10.6	0.52	221	2352.9	45	6.0	<1000	6.0	P
A2-4	13	11.8	0.55	158	3481.0	85	6.3	<1000	6.3	P
A2-4	13OF	11.1	0.55	225	2444.4	80	6.1	1520	6.1	P
A2-4R1	12	9.0	0.55	155	3540.5	15	5.0	2983	5.0	Q
A2-4R1	23	9.6	0.52	141	3675.8	41	5.5	1962	5.5	P
A2-4R1	13	9.6	0.55	138	3976.7	26	5.5	2600	5.5	P
A2-4R1	3SH	9.4	0.50	1112	449.64	NA	NA	NA	NA	NA/W
A2-4R1	2SH	8.2	0.50	1205	414.94	NA	NA	NA	NA	NA/W
A2-4R1	1SH	8.8	0.50	1022	489.24	NA	NA	NA	NA	NA/W
A2-4R2	12	8.3	0.55	155	3548.4	6	5.3	3253	0.6	G
A2-4R2	13	9.4	0.52	160	3250.0	22	5.4	2344	5.4	P/Q
A2-4R2	23	8.2	0.55	161	3416.1	13	5.3	2500	5.3	Q
CP1	12	10.0	0.70	173	4046.2	5	0.3	3390	0.3	G

Table 2.2 Summary of CSL Results at Site 2

Shaft	Tube Pair / log	Test Length (m)	Tube Dist. (m)	FAT Ave (ms)	V_{avg} (m/s)	V_{max} Red. %	Depth V_{max} % M	V_{min} (m/s)	Depth V_{min} (m)	CRC
CP1	13	9.7	0.96	242	3966.9	8	0.0	3296	0.0	G
CP1	14	9.7	0.61	160	3812.5	4	0.5	3466	0.5	G
CP1	23	9.8	0.70	174	4023.0	6	0.8	3576	0.8	G
CP1	24	9.7	0.88	229	3842.8	4	0.3	3451	0.3	G
CP1	34	9.9	0.70	165	4242.4	4	0.0	3697	0.0	G
CP2	12	9.1	0.58	160	3625	5	2.6	3452	8.2	G
CP2	13	8.8	0.91	233	3905.6	8	0.0	3305	0.0	G
CP2	14	9.2	0.73	162	4506.2	3	2.7	4056	0.0	G
CP2	23	9.2	0.70	168	4166.7	5	2.3	3487	0.4	G
CP2	24	8.9	0.91	225	4044.4	5	8.7	3652	0.3	G
CP2	34	9.3	0.67	161	4161.5	9	0.9	3503	0.9	G
CP3	12	10.5	0.70	169	4142	5	3.4	3731	0.5	G
CP3	13	10.5	0.88	215	4093	7	6.3	3735	3.4	G
CP3	14	10.7	0.58	158	3670.9	9	3.4	3177	3.4	G
CP3	23	10.5	0.52	144	3611.1	6	8.9	3192	8.5	G
CP3	24	10.1	0.88	226	3893.8	8	0.4	3408	0.4	G
CP3	34	10.4	0.76	159	4779.9	6	0.0	4318	0.0	G
CP4	12	9.4	0.64	175	3657.1	10	7.6	3206	7.6	G
CP4	13	9.1	0.88	220	4000	7	2.5	3418	0.1	G
CP4	14	9.2	0.58	152	3815.8	7	5.9	3400	5.9	G
CP4	23	9.2	0.67	157	4267.5	5	0.1	3539	0.0	G
CP4	24	9.3	0.88	223	3946.2	7	0.5	3361	0.4	G
CP4	34	9.2	0.61	147	4149.7	6	5.1	3847	7.0	G

Visual inspection of the tubes at the top of the drilled shafts indicated that many of the tubes might not be parallel and might be slightly skewed. Therefore, it was believed that many of the variations in apparent velocity were due to non-uniform

tube spacing rather than variable shaft quality. This is especially true for the logs such as CP4-23 (pier shaft 4, tubes 2-3), which exhibit a gradual sloping change in apparent velocity over a distance of several meters as shown in Figure 2.8. More abrupt changes in arrival time and apparent velocity over shorter distances, with

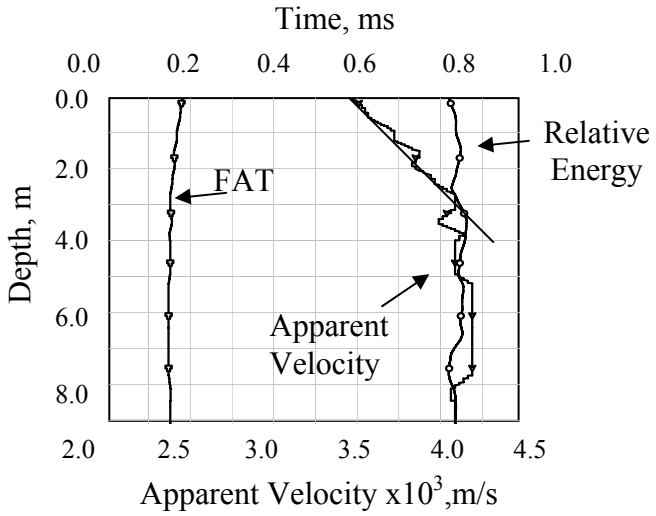

Figure 2.8 Variations in Apparent Velocity Due to Non-Uniform Tube Spacing. CSL Log from CP4 between Tubes 2&3

uniform records above and below, are more likely due to deviations in concrete quality.

During CSL logging, data were recorded from the bottom of the tubes to some elevation above the concrete. Data along the concrete length, as measured during the testing, are plotted, and all other data are removed.

2.2.2.2 CSL Test Results and Analysis

The CSL data were plotted and analyzed according to the concrete condition criteria project specifications. The CSL x,y logs (Appendix B) consist of plots of arrival time, "apparent" velocity, and "relative" energy for all tested shafts.

Based on the CSL results from the first set of tests performed, all abutment drilled shafts with the exception of drilled shaft A2-4 were categorized as G (good) per the ranking system given in the project specifications. This indicates that the logs do not show arrival time signal distortions or arrival time delays that deviate by more than 10% from the average log arrival time.

The CSL record for shaft A2-4, however, indicates a significant delay and signal loss at a depth between 6 and 7 m from the top of the shaft, and was rated as P/D (Poor/Defect). This means that the logs showed a decrease in wave velocity of 20% or more, and that a high probability of concrete defect exists. Abrupt velocity reductions at this depth ranged from about 14% for tube pair 1-2 greater than 50% for tube pair 2-3 and were recorded in both normal and offset logs. Since the maximum signal losses were measured between tubes 2-3 and 1-3, the defect might be centered close to tube number 3. However, the exact geometry and location of the defect is not clear.

The retest of shaft A2-4 (16 days later) was conducted to determine the accuracy of the CSL tests and to evaluate the intensity of the anomaly after further concrete curing. The logs showed similar results with minor reduction in signal delay magnitudes from the previous tests. This indicates that CSL results were accurate, a defect existed at 6 to7 m depth, and further concrete curing had somewhat improved the conditions. CSL logs from both tests are shown in Figure 2.9. The figure shows that the signal delays in the event logs had been reduced from about 14%, 29%, >50% after test 1 to 5%, 25% and 32% after test 2 for tube pairs 1-2, 1-3, and 2-3, respectively.

Difference tomograms between the signals obtained from pre-grouting *Test 1* and *Test 2* were also calculated and are presented in Figure 2.10, as three sets of tomograms representing crosscuts between access tubes. The first tomogram of each

set shows a 3-D rotated image of the areas with signal improvement of at least 500 m/s. The second tomogram of each set shows 2-D cross-sectional difference in signal improvement between both pre-grouting tests. The figures depict areas (red colored) of signal improvement up to 1000 m/s.

2.2.2.3 Tomographic Imaging of the CSL Test Results

Based on both CSL test results, it became obvious that a significant zone of deficient concrete existed in A2-4, and immediate remediation was required. Obtaining core samples from the anomalous zone to physically inspect the concrete, to confirm actual location, and to grout encountered deficient zones was the obvious solution. Since the CSL logs did not indicate the size, geometry, and severity of the defect, it was difficult to recommend a placement location for the 50-mm-diamter core holes. A 3-D velocity tomographic analysis of the A2-4 shaft using the CSL data produced a clear image of the geometry and location of the anomaly as shown in Figure 2.11. The average ultrasonic apparent velocity was calculated to be approximately 3,660 m/s. The 3-D images indicated most of the area within the shaft had a velocity greater than the average, indicating sound concrete. The zones with velocity contours of 10% (velocity of 3,294 m/s in green) and 20% (velocity of 2,928 m/s in blue) reduction were plotted. A minor zone of about 10% reduction was depicted in the upper part of the shaft between 0.5 and 2.5 m, and a 20% reduction zone that extended across the entire shaft diameter was depicted between 6.6 and 7.5 m depth. After reviewing the tomographic images, the defects within shaft A2-4 were located on top of the shaft and two core holes were drilled. Concrete core samples were retrieved for physical investigation and evaluation. The core holes were drilled at the abutment 2 shaft 4 in between tubes 1-3 and 2-3 perpendicular to the line in between tubes from their middle point, and in the outside of the tubes triangle. The 50-mm-diameter core holes were drilled 150 mm from the spiral rebar cage perpendicular to

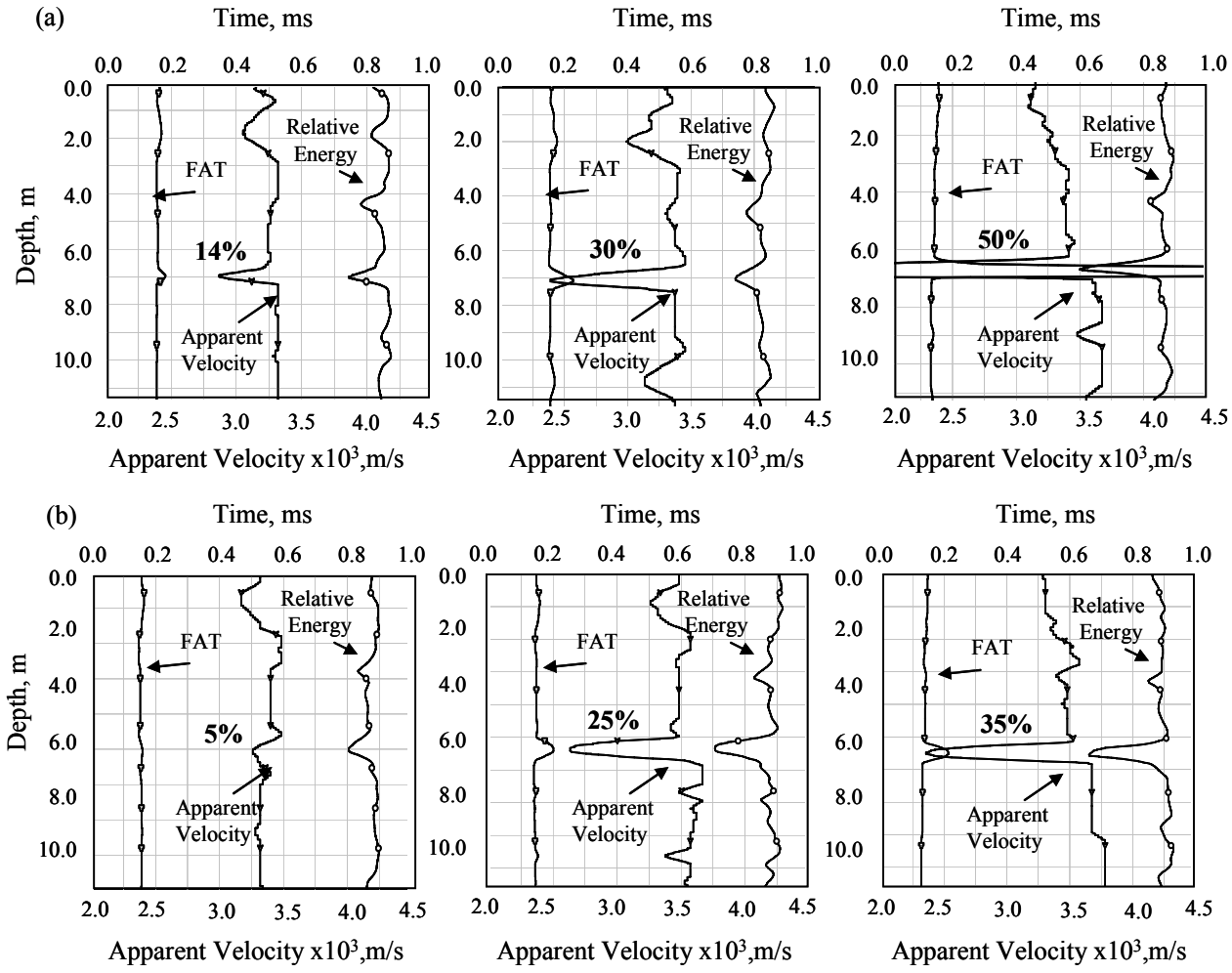

Figure 2.9 (a) Initial CLS Test of the A2-4, (b) CSL Test of the A2-4 After 16 Days of Curing

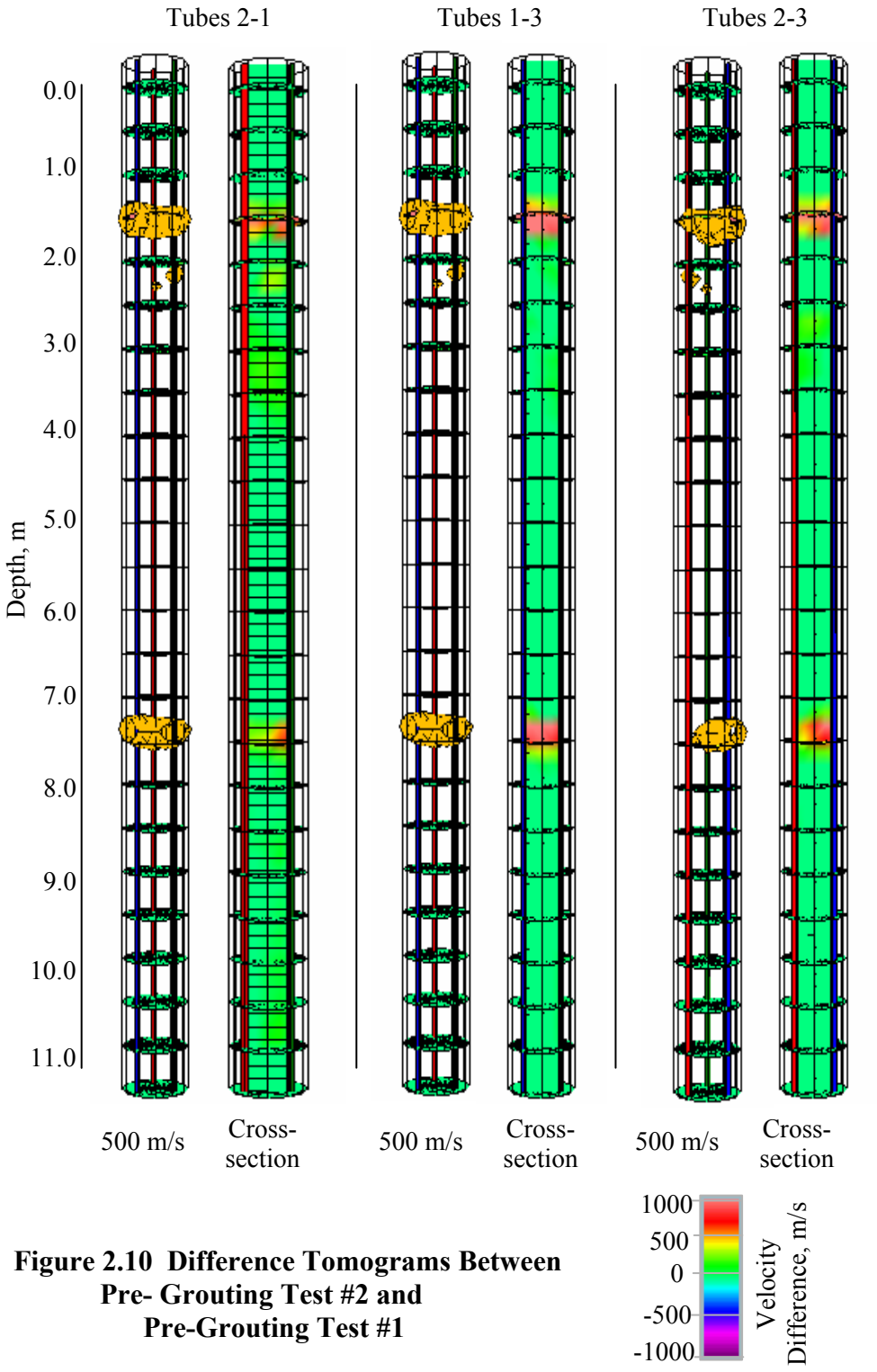

Figure 2.10 Difference Tomograms Between Pre- Grouting Test #2 and Pre-Grouting Test #1

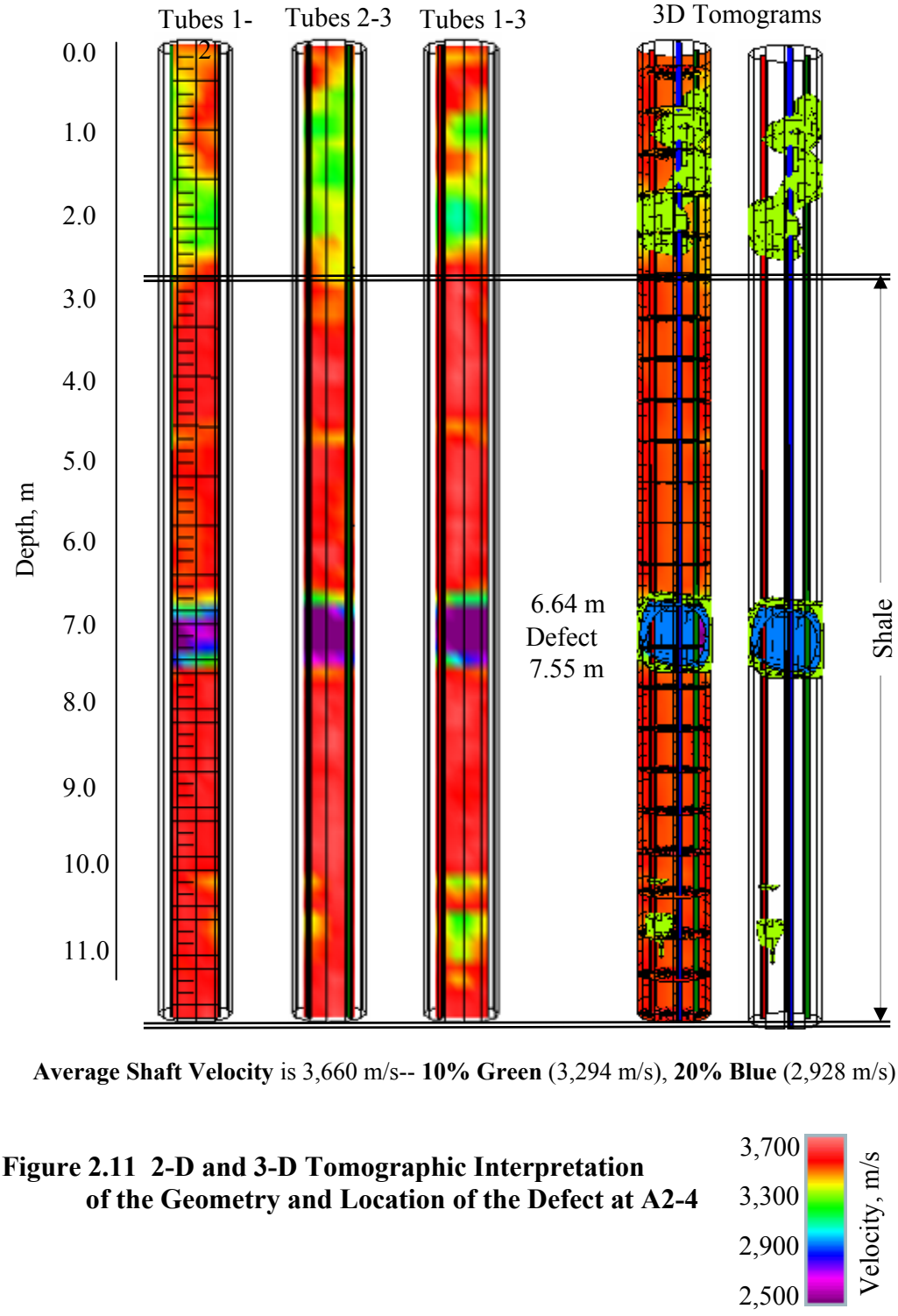

Average Shaft Velocity is 3,660 m/s-- **10% Green** (3,294 m/s), **20% Blue** (2,928 m/s)

Figure 2.11 2-D and 3-D Tomographic Interpretation of the Geometry and Location of the Defect at A2-4

the middle point of the line in between tube pairs 1-3 and 2-3, as shown in Figure 2.12. The coring procedure is presented in Figure 2.13. The southeast (SE) core hole (between tube pairs 2-3) was advanced to a depth of 8.38 m and southwest (SW) (between tube pairs 1-3) was advanced to a depth of 9.14 m. At each location, extracted cores resulted in numerous mechanical fractures of the core as shown in Figure 2.14. Most of these fractures are attributed to hammering on the core barrel while extracting the core from the barrel. Since the core spins as the drill rotates, determining core orientation is not possible. The coring results were logged, and the cores were photographed.

Core inspection indicated that no defective concrete was encountered during coring in the core hole between tubes 2-3. However, the core hole between tube 2-3 encountered a weak zone, 0.15 m long, at about 6.5 m from the top of the shaft. The anomaly consisted of a pocket of well-graded, yellow-brown sand in one-half of the core. The sand pocket abruptly terminated in good concrete. Below the sand pocket, the core contained mechanical fractures resulted in a short 50-mm section of somewhat more competent concrete core that represents the last few millimeters of core run #7. Core runs #8 and #9 were all in good uncontaminated concrete. The orientation of the sand pocket could not be ascertained. A low-density concrete zone was also encountered between 1 m and 2 m from the top of the shaft as indicated in the tomograms. This zone was not of concern.

Although a weak sand pocket existed at the predicted depth, coring results did not indicate the anomaly zone with the same size and intensity as was recorded by the CSL testing and tomography imaging. This discrepancy might have been due to vertical CSL tube deviation or because the standard 20% deviation in the velocity was not correct.

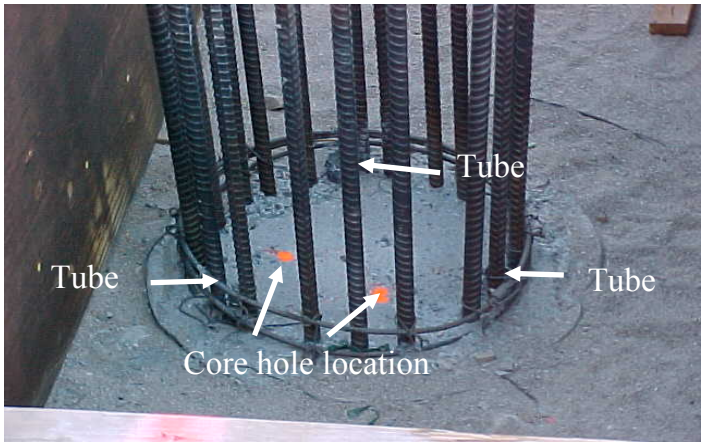

Figure 2.12 Location of the Coreholes and CSL Tubes of the A2-4

Figure 2.13 Coring Procedure of the A2-4 at Site # 2 Bridge

Further analysis of the CSL data with the 3-D tomography techniques was conducted to determine the percent in velocity deviation that should have been contoured to match the coring results. The data were reprocessed, and a close-up image was plotted of the zone between 6.5 and 7.5 m depth. The projection of the two core-holes showing contours of the 20%, 30%, and 50 % reduction in velocity is shown in Figure 2.15 and Figure 2.16. From the figures, it can be seen that the sand pocket coincided with the 30% velocity reduction, and not the 20% as specified in the guidelines.

2.2.2.4 Pile Repair Procedure

A pile repair procedure was developed with the objective to improve the defect zone in the A2-4 drilled shaft. Permeation grouting to improve the strength and reduce permeability of the low-density zones within the shaft was recommended. Permeation grouting has been effective in the past to improve the concrete density and the density of the granular soil around and below the drilled shaft to improve resistance capacity. Pressure grouting is a process where a suspension of super-fine cementations slurry or resin grout is pumped under a predetermined pressure into a porous material. The grout will penetrate the pores, harden, and become a permanent part of the material matrix. Drilled shaft repair at this Bridge was done using Fosrock Ultracem grout. As a general rule for effective grouting, the minimum diameter opening that suspended cement particles will enter is five times the effective cement grain size.

During pressure grouting, packers were installed and seated in the core hole between tubes 1-2 at a depth of a few meters above the top of the zone of deficient concrete. A pressure gage was located near the grout plant to monitor the pressure in the sealed holes. Water was injected to test the seating of the packer and to flush the sand out of the grout zone. The pressure quickly reached 3.5 MPa and was maintained for a

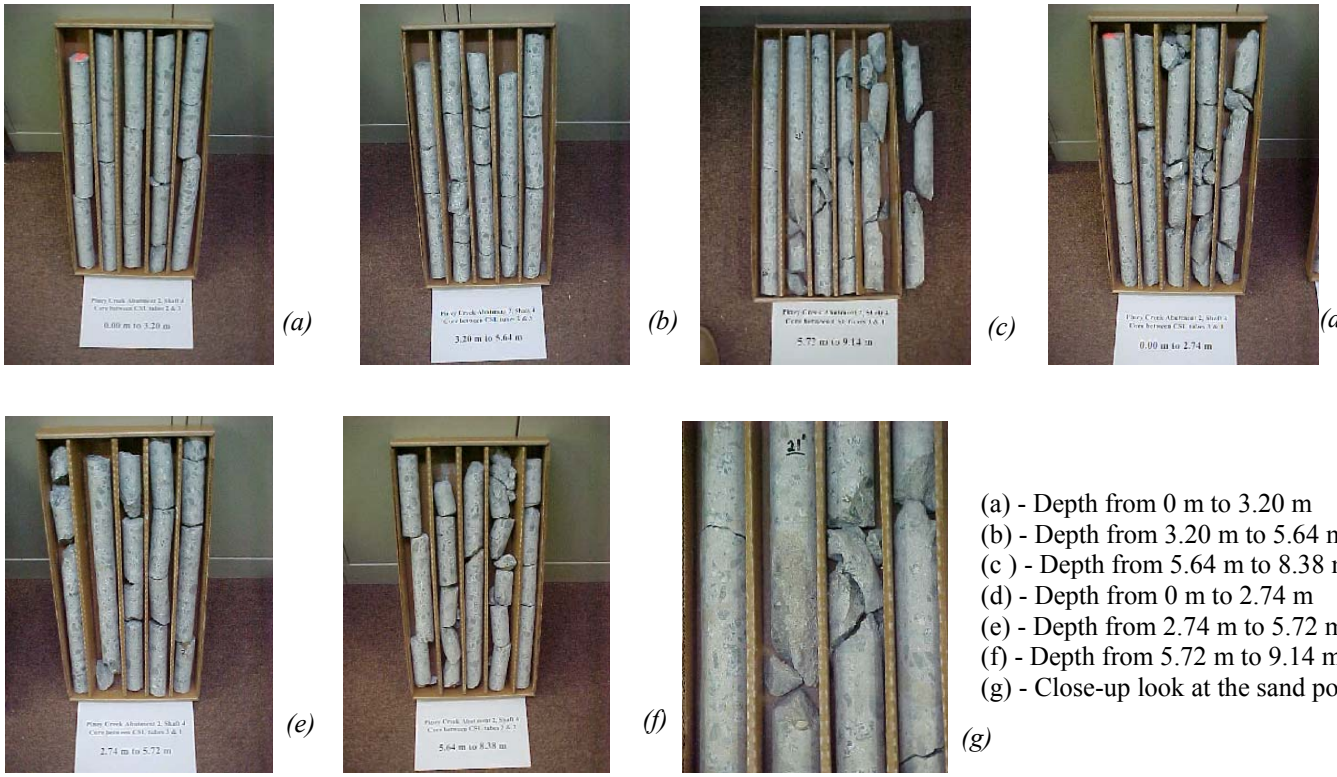

(a) - Depth from 0 m to 3.20 m
(b) - Depth from 3.20 m to 5.64 m
(c) - Depth from 5.64 m to 8.38 m
(d) - Depth from 0 m to 2.74 m
(e) - Depth from 2.74 m to 5.72 m
(f) - Depth from 5.72 m to 9.14 m
(g) - Close-up look at the sand pocket

Figure 2.14 (a-c) Cores from the SE Core Hole (in Between CSL Tubes 2-3) and (d-g) Cores from the Corehole in-between CSL Tubes 1-3 of the A2-4 Drilled Shaft for "Site 2 Bridge

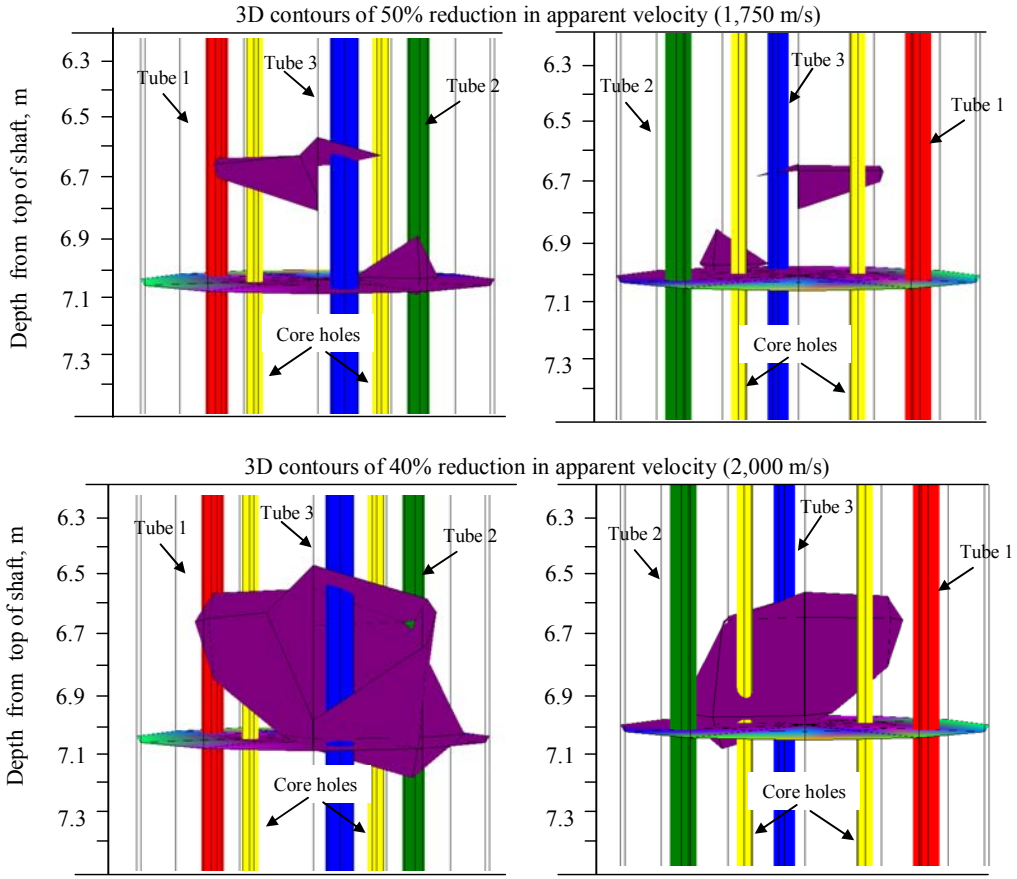

Figure 2.15 Close-Up Look at the Defect with Velocity Reduction Counters (30% & 50% Reduction)

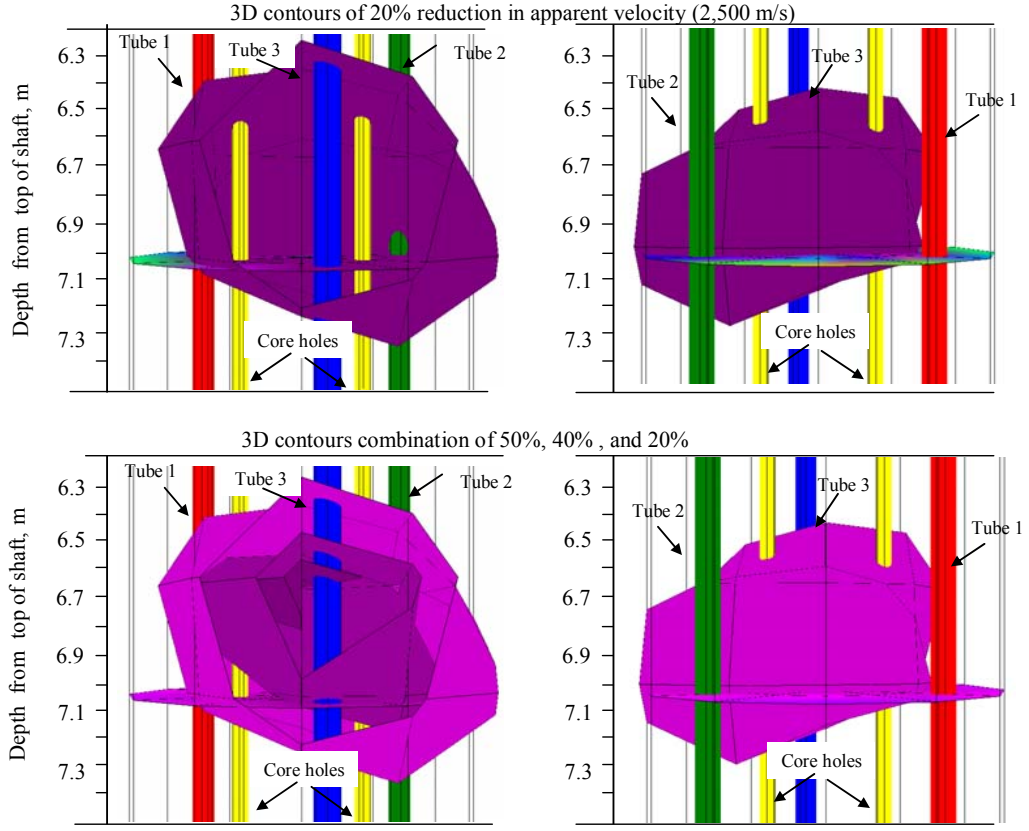

Figure 2.16 Close-Up Look at the Defect with Velocity Reduction Counters (20% Reduction and Combination of all)

certain period of time. No connections with the other core hole or the outside of the shaft were noticed. This confirms that no weak zones that may require grouting were encountered. This hole was then filled with grout to the top of the shaft. Figure 2.17 shows the mechanism that was used during the grouting procedure. Difference tomograms between the signals obtained from pre-grouting (Test 2) and post-grouting were calculated and are presented in Figure 2.18 as three sets of tomograms representing cross-sections between access tube pairs. The first tomogram of each set shows areas of velocity improvement of at least 500 m/s in 3-D contours. The second tomogram of each set shows 2-D cross-sectional differences in velocity improvement between pre- and post-grouting tests. The figures depict areas (red) of signal improvement up to 1,000 m/s caused by grouting. The same procedure was performed in the core hole between tubes 2-3. However, no pressure was measured during packer testing even though about 100 gallons of water were pumped into the hole. This indicates that a significant defect existed at this depth. It was also determined that there was contact through to the outside of the shaft. Therefore, the contractor wanted to clean out as much of the fines in the decomposing shale as possible and remove all the sand from the shaft. Almost all of the grout material was used to fill the core holes and build the required 3.5 Mpa pressure.

After the successful grouting of the A2-4 shaft, CSL retesting was performed using the standard procedures. Initial measurements of the depth of the tubes indicated tubes 1 and 3 were approximately 10.4 m deep, whereas tube 2 was initially 9.1 m. Dropping the weight at the end of the measuring tape to the bottom apparently compacted the soft bottom or caused some of the sediment at the bottom of the tube to go into suspension. When testing began, the depth to the bottom of tube 2 was 9.3 m. When testing cross-sections 1-2 and 2-3, the bottom of tube 2 was used as a starting point for both transducers.

The CSL retest results (after repair), Figure 2.19, indicated a minor signal velocity reduction at a depth of approximately 6 m from the top. These velocity reductions ranged

(a) (b)

Figure 2.17 (a) & (b) Mechanism Used for Pressure Grouting

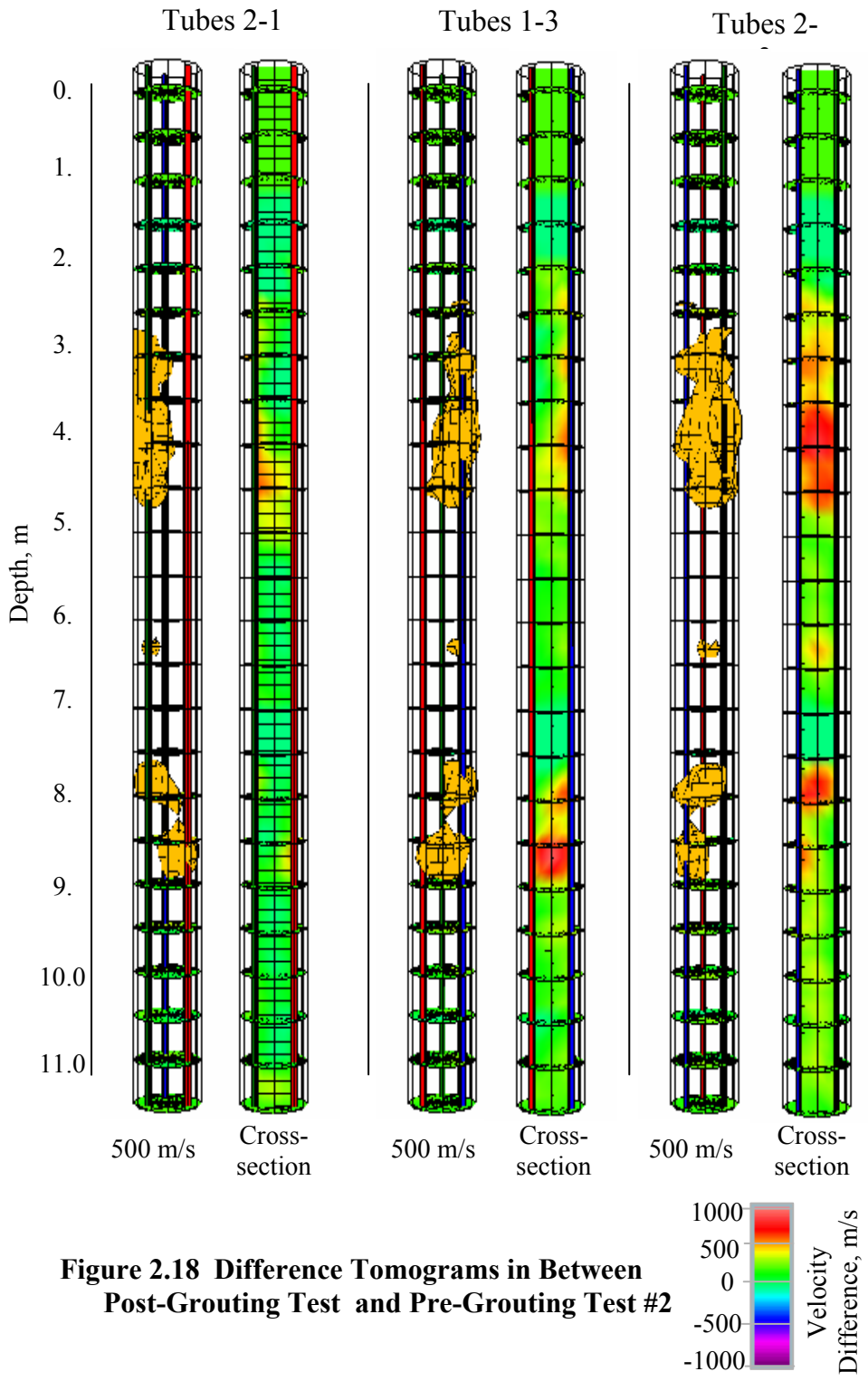

Figure 2.18 Difference Tomograms in Between Post-Grouting Test and Pre-Grouting Test #2

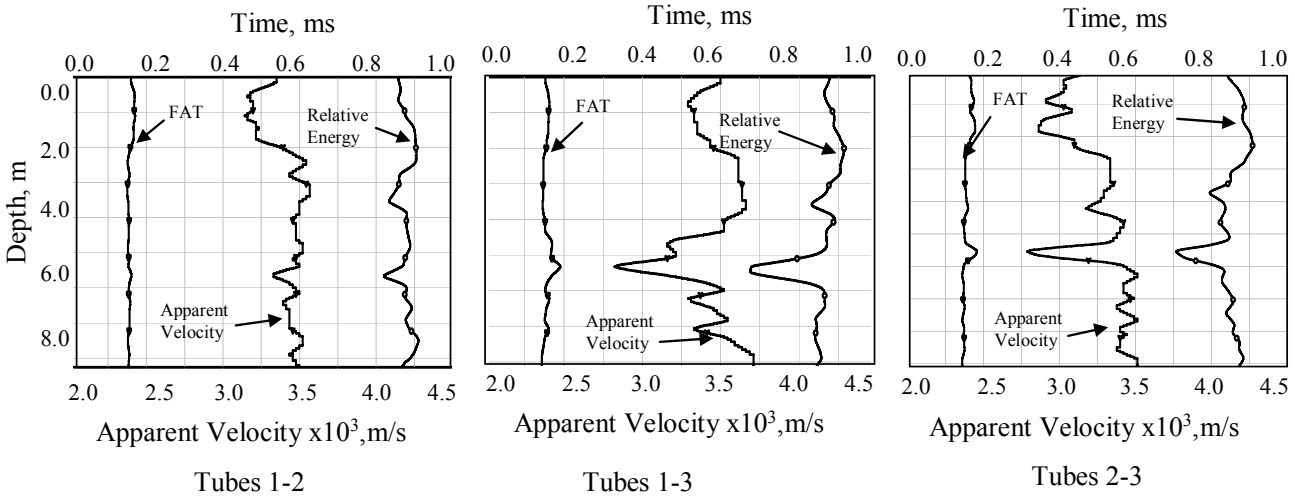

Figure 2.19 CSL Retest Results After Pressure Grouting

from 7% for tube pair 1-2 to about 16% for tube pairs 1-3 and 2-3. The average velocity was estimated at 3,800 m/s for pairs 1-2 and 2-3, and 3,900 m/s for pair 1-3. The results indicate that the grouting procedure had improved the concrete density within the anomalous zone and reduced the intensity of the defect, but did not completely eliminate the defect. Based on the retest results and the location of the defect within the drilled shaft, the drilled shaft was acceptable for further bridge construction.

2.3 Tomographic Imaging Summary and Recommendations

Several conclusions were derived from these field investigations:

1. The cross-hole sonic logging method, despite certain limitations is; (a) a valid and conclusive technique in assessing the integrity of deep concrete foundations; (b) is flexible and economical for use in deep shafts; (c) is accurate and repeatable but highly sensitive to measurement errors; for example, relatively minor deviations of a tube can introduce significant deviation in the "*first arrival time"* picks that are related to the dynamic property of the medium as "apparent" velocity; (d) is capable of locating structural defects and detecting velocity variations within a medium; and, (e) is a two-dimensional method, which makes it difficult to interpret the results in terms of size and geometry of defects or lateral (in vertical cross-section perspective) variations in velocity distribution.
2. Accurate interpretation of CSL results is an important issue in evaluating the integrity of deep foundations. Tomography is a method that may overcome the limitations in CSL concerning the interpretation of results. Three-dimensional color-coded tomographic imaging adds an advantage to the CSL system output by allowing imaging the location, size, and geometry of a defect with high accuracy.

3. Tomography software separates and presents certain specific velocities representing various questionable zones of defect geometry with high resolution.

4. An important advantage of tomography is the capability to provide a visual image of lateral variations in velocity within a structure. The process is capable of determining inter-tube velocity variations of 5% or better.

5. Zero probe-offset data produce the highest range of velocities because of the smaller path length during the CSL data collection. Best aperture and therefore highest image resolution converges when combining rays from several offsets. For tomography, CSL data collection with offsets may be more effective for accurately imaging concrete structures.

6. Tomography research on the Site #2 Project has shown no-analogy between the CSL test results, tomographic interpretation, and coring results. For this case study, CSL data collection was performed four different times on the same shaft (initial test, test with the offsets, retest after 16 days of curing, and retest after pressure grouting). In each case, the CSL data detected the defect on the same horizon, but with some improvement followed by the pile repair procedure. Based on the coring results, the defect within the shaft corresponded better to a 30% increase in velocity than to a 20% increase.